Parameterizing Eddy-Induced Tracer Transports in Ocean Circulation Models

PETER R. GENT

National Center for Atmospheric Research, Boulder, Colorado

JURGEN WILLEBRAND

Institut für Meereskunde an der Universität Kiel, Kiel, Germany

TREVOR J. MCDOUGALL

CSIRO Division of Oceanography, Hobart, Australia

JAMES C. MCWILLIAMS

National Center for Atmospheric Research, Boulder, Colorado

(Manuscript received 23 August 1993, in final form 20 January 1994)

ABSTRACT

It is shown that the effects of mesoscale eddies on tracer transports can be parameterized in a large-scale model by additional advection and diffusion of tracers. Thus, tracers are advected by the effective transport velocity, which is the sum of the large-scale velocity and the eddy-induced transport velocity. The density and continuity equations are the familiar equations for adiabatic, Boussinesq, and incompressible flow with the effective transport velocity replacing the large-scale velocity. One of the main points of this paper is to show how simple the parameterization of Gent and McWilliams appears when interpreted in terms of the effective transport velocity. This was not done in their original 1990 paper. It is also shown that, with the Gent and McWilliams parameterization, potential vorticity in the planetary geostrophic model satisfies an equation close to that for tracers. The analogy of this parameterization with vertical mixing of momentum is then described.

The effect of the Gent and McWilliams parameterization is illustrated by applying it to a strong, sloping two-dimensional front. The final state is that the front is flat, corresponding to a state of minimum potential energy. However, the amount of water of a given density has not been changed and there has been no flow across isopycnals. These properties are not preserved with horizontal diffusion of tracer. Finally, the Levitus dataset is used to estimate the effects of the Gent and McWilliams parameterization. The zonal mean meridional overturning streamfunction for the eddy-induced transport velocity has a maximum of 18 Sverdrups near the Antarctic Circumpolar Current. The associated poleward heat transport is 0.4 petawatts. The maximum poleward heat transport in the Northern Hemisphere is 0.15 petawatts at 40°N. These values are the same order of magnitude as estimates from observations and regional eddy-resolving ocean models.

1. Introduction and rationale in isopycnal coordinates

Increasing computing power has meant that eddy-resolving ocean general circulation calculations that integrate for several decades are now quite feasible. However, the deep ocean takes at least several hundred years to come into equilibrium, and many calculations that thoroughly explore parameter space are desirable. This means that, at the present time, most ocean components of climate models use a coarse resolution that does not resolve ocean eddies. Thus, the effects of eddies need to be parameterized in these models and it has proved difficult to accomplish this satisfactorily.

One reason is that the most obvious and simplest parameterization, downgradient Fickian diffusion, has been demonstrated to be inadequate. A major reason for this inadequacy is that a purely diffusive parameterization means that advection in the large-scale model is by the large-scale velocity. Observational and numerical model studies, especially of the stratosphere as well as the ocean, have clearly shown that, on average, tracers are not advected by the large-scale velocity. This can be demonstrated as follows.

Consider incompressible, Boussinesq, and adiabatic flow in isopycnal coordinates. We will also assume that the equation of state for seawater is a linear function of potential temperature and salinity with constant coefficients. The density and continuity equations are combined to give an equation for the thickness h_ρ,

Corresponding author address: Dr. Peter Gent, NCAR, P.O. Box 3000, Boulder, CO 80307-3000.

where ρ is the density and $h(x, y, \rho, t)$ is the physical height of a density surface. The equation is

$$\frac{\partial}{\partial t} h_\rho + \nabla_\rho \cdot (h_\rho \mathbf{u}) = 0, \tag{1}$$

where $\mathbf{u}$ is the horizontal velocity vector and ∇_ρ is the horizontal gradient operator applied at constant ρ. The equation for the conservation of a tracer τ is

$$\frac{\partial}{\partial t} (h_\rho \tau) + \nabla_\rho \cdot (h_\rho \mathbf{u} \tau) = 0. \tag{2}$$

If the variables are decomposed into large-scale components denoted by an overbar and eddy components denoted by primes by a low-pass projection operator in time and space at constant density, then the thickness equation (1) becomes

$$\frac{\partial}{\partial t} \overline{h_\rho} + \nabla_\rho \cdot (\overline{h_\rho} \bar{\mathbf{u}} + \overline{h'_\rho \mathbf{u}'}) = 0, \tag{3}$$

and the tracer equation (2) becomes

$$\frac{\partial}{\partial t} (\overline{h_\rho} \bar{\tau} + \overline{h'_\rho \tau'}) + \nabla_\rho \cdot (\overline{h_\rho} \bar{\mathbf{u}} \bar{\tau} + \overline{h'_\rho \mathbf{u}'} \bar{\tau}) = -\nabla_\rho \cdot [\overline{(h_\rho \mathbf{u})' \tau'}]. \tag{4}$$

Using (3), Eq. (4) can be written in the form

$$\frac{\partial}{\partial t} \bar{\tau} + \frac{1}{\overline{h_\rho}} \frac{\partial}{\partial t} (\overline{h'_\rho \tau'}) + [\bar{\mathbf{u}} + (\overline{h'_\rho \mathbf{u}'})/\overline{h_\rho}] \cdot \nabla_\rho \bar{\tau} = -\nabla_\rho \cdot [\overline{(h_\rho \mathbf{u})' \tau'}]/\overline{h_\rho}. \tag{5}$$

Equations (3) and (5) are for the large-scale thickness and large-scale tracer, which involves eddy-correlation terms.

Equations for the large-scale model are now formulated based on these equations and insight into the form and parameterization of the eddy terms. It is assumed that the eddy components of thickness and tracer are uncorrelated so that the second term in Eq. (5) is neglected in the large-scale model tracer equation. Another fundamental assumption is that ocean eddies mix tracers along isopycnals and not across them so that the right-hand side of (5) can be parameterized as Fickian diffusion along isopycnals with coefficient μ. Thus, we choose the large-scale model tracer equation, based on (5), to be

$$\frac{\partial}{\partial t} \tau + \mathbf{U} \cdot \nabla_\rho \tau = \nabla_\rho \cdot (\mu h_\rho \nabla_\rho \tau)/h_\rho, \tag{6}$$

where overbars have been dropped because the quantities in Eq. (6) are large-scale model variables. Note that the mixing along isopycnals term on the right-hand side of (6) involves the approximation of small isopycnal slopes (see page 151 of Gent and McWilliams 1990). Equation (6) says that model tracers are advected along isopycnals by a velocity $\mathbf{U}$, and there is a formal identification between Eqs. (5) and (6) with

$$\mathbf{U} = \bar{\mathbf{u}} + (\overline{h'_\rho \mathbf{u}'})/\overline{h_\rho}. \tag{7}$$

The large-scale model thickness equation, based on (3), can also be written in terms of $\mathbf{U}$ as

$$\frac{\partial}{\partial t} h_\rho + \nabla_\rho \cdot (h_\rho \mathbf{U}) = 0. \tag{8}$$

A specification of $\mathbf{U}$ in terms of large-scale model variables, based on a parameterization of the eddy-correlation term in (7), is made in section 3.

De Szoeke and Bennett (1993) also address the question of averaging the equations of motion. They average over microscopic scales and then transform into coordinates relative to the microscopically averaged isopycnals. They address parameterization of the microstructure fluxes that arise in this averaging process. We do not address this issue, and the coordinates in this section should be thought of as the microscopically averaged coordinates of de Szoeke and Bennett (1993). They do not address the parameterization of mesoscale eddy fluxes, which is the subject of this work. They propose that the equations of motion be formulated in terms of $\mathbf{U}$ defined in (7) above, which they call the thickness-weighted average horizontal velocity. However, this requires parameterization of Reynolds stress terms in the momentum equation, and we restrict our attention to tracer and density fluxes. Nevertheless, in section 4 we formulate the planetary geostrophic momentum equation in terms of $\mathbf{U}$ in order to show an analogy with vertical mixing of momentum.

The fact that the large-scale model tracers in (6) are not advected by the large-scale velocity alone has been well documented in the atmospheric science literature, especially in connection with tracer transports in the stratosphere. The atmospheric scientists have defined several different two-dimensional circulations in the meridional and vertical plane that apply to zonally averaged quantities. They are clearly and thoroughly discussed in the book on middle atmosphere dynamics by Andrews et al. (1987). Plumb and Mahlman (1987) diagnosed the zonally averaged tracer transports in the GFDL general circulation/transport model and used the name "effective transport velocity" for the velocity advecting the tracers. As noted by Plumb and Mahlman, the effective transport velocity is not, in general, the "Lagrangian-mean velocity" of Andrews and McIntyre (1978) when the diffusivity is spatially inhomogeneous. When this occurs, as it should in ocean circulation models, then the Lagrangian-mean and effective transport velocities differ by the gradient of the diffusivity. Plumb and Mahlman also note that the effective transport velocity satisfies the usual continuity equation, whereas the Lagrangian-mean velocity does not. The large-scale model formulated above is three-

dimensional, and the concept of effective transport velocity is valid in this situation as well. Contributions in this vein have been made by Plumb (1986, 1990) and Andrews (1990). There have been at least two names used for the eddy-correlation term in Eq. (7) in the oceanographic literature. Rhines (1982) and McDougall (1991) used bolus velocity, while Csanady (1989) used peristaltic pumping velocity. We prefer "eddy-induced transport velocity."

The eddy contribution to the tracer equation can be written quite generally as a 3×3 tensor operating on the gradient of the tracer. This tensor can be written as the sum of a symmetric component and a skew-symmetric component that is antisymmetric about the diagonal. The symmetric component is a diffusion operator, which can be written in purely diagonal form in some coordinate system. We have assumed above that this symmetric component is diagonal in coordinates lying along and normal to isopycnal surfaces. The skew-symmetric component can alternatively be written as an advection, which we have assumed is along isopycnals and not normal to them. This view of eddy effects on tracers has been discussed previously by Middleton and Loder (1989) and recently by Davis (1994).

2. Transformation to height coordinates

In section 1 it was assumed that the large-scale model tracer fields are advected along isopycnals by $\mathbf{U}$ and there is no advection across isopycnals. In height coordinates this is achieved by defining the three-dimensional effective transport velocity $(\mathbf{U}, W)$ such that

$$\frac{D^*}{Dt}\rho = \frac{\partial}{\partial t}\rho + \mathbf{U}\cdot\nabla\rho + W\rho_z = 0, \qquad (9)$$

where D^*/Dt is the substantial derivative that advects with the effective transport velocity, and ∇ is the two-dimensional gradient operator at constant height. The eddy-induced transport velocity $(\mathbf{u}^*, w^*)$ is defined by

$$\mathbf{U} = \mathbf{u} + \mathbf{u}^*, \quad W = w + w^*, \qquad (10)$$

where $(\mathbf{u}, w)$ is the large-scale velocity. Other large-scale model equations can be written in terms of $(\mathbf{u}, w)$, which is the Eulerian velocity of the large-scale model. Based on the analogy in section 1, this velocity represents an observed velocity that has been filtered by a low-pass projection operator in time and space at constant density. The transformed tracer equation (6) takes the form

$$\frac{D^*}{Dt}\tau = R(\mu, \tau), \qquad (11)$$

where $R(\mu, \tau)$ is the transformation of the right-hand side of (6), namely

$$R(\mu, \tau) = \nabla^{3D}\cdot[\mu\mathbf{K}\nabla^{3D}\tau]. \qquad (12)$$

The 3×3 tensor $\mathbb{K}$ and the two-dimensional slope vector $\mathbb{L}$ are given by

$$\mathbb{K} = \begin{pmatrix} \mathbb{I} & \mathbb{L} \\ \mathbb{L} & \mathbb{L}\cdot\mathbb{L} \end{pmatrix}, \quad \mathbb{L} = -\nabla\rho/\rho_z, \qquad (13)$$

and $\mathbb{I}$ is the 2×2 identity matrix. Here $\mathbf{K}$ is the small slope form for isopycnal mixing given in Cox (1987) and Eq. (22) of Gent and McWilliams (1990). It is now easy to deduce from (8) and (9) that the effective transport velocity and, hence, the eddy-induced transport velocity both satisfy the usual continuity equation, namely

$$\nabla\cdot\mathbb{U} + W_z = \nabla\cdot\mathbf{u}^* + w_z^* = 0. \qquad (14)$$

In the ocean the eddy fluxes are zero at closed boundaries, so that the normal component of the eddy-induced transport velocity is zero on closed boundaries. Thus,

$$(\mathbb{U} + W\mathbf{k})\cdot\mathbf{n} = (\mathbf{u}^* + w^*\mathbf{k})\cdot\mathbf{n} = 0, \qquad (15)$$

where $\mathbf{k}$ is the unit vertical vector and $\mathbf{n}$ is the unit vector normal to the boundaries.

Equations (9), (11), (14), and (15) are the familiar equations for adiabatic, Boussinesq, incompressible flow but with the effective transport velocity replacing the large-scale velocity. The three properties listed by Gent and McWilliams (1990) as important to retain in any parameterization can be deduced from these equations immediately. The properties are

1) all domain-averaged moments of ρ are conserved and the volume between any two isopycnals is conserved;

2) with insulating boundary conditions, the domain-average of τ is conserved between any two isopycnals, and higher moments of τ decrease in time if τ has gradients on the isopycnals;

3) the tracer equation (11) is satisfied identically by the density, ρ.

One of the main points of this paper is to show how simple the formulas in Gent and McWilliams (1990) appear when interpreted as above in terms of the effective transport velocity. Equations (9) and (11) show that there is no movement of tracers across isopycnal surfaces, and there is no diapycnal velocity in this parameterization. It is clear that any diapycnal velocity should be calculated with respect to the effective transport velocity $(\mathbb{U}, W)$ and not with respect to the large-scale velocity $(\mathbb{u}, w)$. Gent and McWilliams (1990) wrote the density and tracer equations, (17) and (19) respectively in their paper, in terms of the large-scale velocity. From their Eq. (19) the eddy-induced transport velocity can be written in their notation as

$$\mathbb{u}^* = \rho_z\mathbb{F}, \quad w^* = -\mathbf{F}\cdot\nabla\rho - Q/\rho_z. \qquad (16)$$

Substitution of (16) into the density equation (9) gives the large-scale velocity form of the density equation, Eq. (17) of Gent and McWilliams (1990), namely

$$\frac{D}{Dt}\rho = \frac{\partial}{\partial t}\rho + \mathbf{u}\cdot\nabla\rho + w\rho_z = Q. \qquad (17)$$

De Szoeke and Bennett (1993) interpret Gent and McWilliams (1990) as a parameterization of diffusion and say "that downgradient flux of density cannot be guaranteed." As stated above, one of the main points of this paper is to show that the Gent and McWilliams (1990) parameterization should be interpreted as a quasi-adiabatic *advection.*

So far, a parameterization choice for the eddy-induced transport velocity has not been made. Any choice that satisfies the boundary condition (15) will satisfy the three properties listed above. This choice could be based on analysis of eddy-resolving calculations, although this has not been attempted here.

3. The Gent and McWilliams (GM90) parameterization

Gent and McWilliams (1990) proposed the following parameterization for the eddy-induced transport velocity:

$$\mathbf{u}^* = -(\kappa\mathbf{L})_z, \quad w^* = \nabla\cdot(\kappa\mathbf{L}), \qquad (18)$$

where κ is the thickness diffusivity, and the vector slope $\mathbf{L}$ is defined in (13). The form for a general vertical coordinate is given in the appendix. This choice is based on the mechanism of nearly downgradient Fickian diffusion of thickness in isopycnal coordinates. The nearly Fickian form was chosen so that w^* can be evaluated as a local function of ρ and, more importantly, because it results in a sign-definite sink of domain-averaged potential energy. This can be seen from the equation for potential energy $g\rho z$,

$$\frac{D^*}{Dt}(g\rho z) = \nabla\cdot(g\rho\kappa\mathbf{L}) + g\rho w + g\kappa\frac{\nabla\rho\cdot\nabla\rho}{\rho_z}. \qquad (19)$$

McWilliams and Gent (1994) chose to satisfy the boundary condition (15) by setting the normal component of $\kappa\mathbf{L}$ to zero on side boundaries and κ to zero on the top and bottom boundaries. Note that this side boundary condition is to be interpreted not as an extra condition on ρ but as a constraint on the discrete form of (18). This side boundary condition also assures that if Eq. (19) is integrated over the domain, the first term on the right-hand side integrates to zero so that it cannot be a source of potential energy. Then the domain-averaged potential energy has the usual transfer to kinetic energy term plus a sign-definite internal sink. This sink of potential energy mimics the domain-averaged effect of baroclinic instability in an eddy-resolving model. This effect is discussed in McDougall and Church (1986) and maintains the properties listed in section 2.

If a model boundary is an open ocean boundary rather than a closed boundary, however, then an alternative specification of (15) may well be more appropriate. This could be to specify a nonzero normal component of $\kappa\mathbf{L}$ on the boundary, which is equivalent to specifying a nonzero normal component of the eddy-induced transport velocity there. In this case, the first term on the right-hand side of (19) can be a source of potential energy, and this possibility is discussed further in section 7.

We now consider potential vorticity in the planetary geostrophic model, which is also often called the thermocline equations in oceanography. The inviscid momentum equation in this model is just a balance between the Coriolis force and the pressure gradient, that is,

$$f\mathbf{k}\times\mathbf{u} + \nabla p/\rho_0 = 0. \qquad (20)$$

The potential vorticity in this model is $f\rho_z$, which is that component of the primitive equation potential vorticity that does not involve velocities. With the GM90 parameterization, the potential vorticity equation can be written as

$$\frac{D^*}{Dt}(f\rho_z) = R(\kappa f, \rho_z) + \nabla\cdot(f\kappa_z\nabla\rho) - \left(f\kappa_z\frac{\nabla\rho\cdot\nabla\rho}{\rho_z}\right)_z. \qquad (21)$$

Equation (21) shows that the potential vorticity is being advected by the effective transport velocity and has mixing of ρ_z along isopycnals with a coefficient κf. The other terms on the right-hand side of (21) are proportional to κ_z and redistribute potential vorticity within the fluid. Boundary condition (15) cannot assure zero boundary fluxes in these terms.

A slightly different parameterization for the eddy-induced transport velocity could be based on exact Fickian diffusion of thickness in isopycnal coordinates. This gives

$$\mathbf{u}^* = -\kappa\mathbf{L}_z, \qquad (22)$$

rather than the GM90 parameterization given in (18). It is interesting to note that with the parameterization (22), the last two terms on the right-hand side of (21) are not present. Then the potential vorticity in the planetary geostrophic model would obey an equation close to that for a tracer (11). The important differences are that (i) the mixing coefficient is proportional to κ rather than to μ and, in general, these two coefficients can have different values and (ii) the mixing acts on ρ_z with f in the coefficient rather than on the potential vorticity. This last feature is desirable because it allows Eq. (21) to have a steady, motionless solution with ρ independent of the horizontal coordinates, whereas mixing of potential vorticity with mixing coefficient κ does not.

Thus, the assumption of exact Fickian diffusion of thickness means that the equation for potential vorticity in the planetary geostrophic model is close to that for tracers.

4. The analogy with vertical mixing of momentum

With the GM90 parameterization, the planetary geostrophic momentum equation (20), including forcing by the wind stress $\mathbf{X}$, can be written in the form

$$f\mathbf{k}\times\mathbf{U}+\nabla p/\rho_0=\left(\kappa f\mathbf{k}\times\frac{\nabla\rho}{\rho_z}\right)_z+\mathbf{X}_z/\rho_0. \quad (23)$$

If the approximation that $\nabla\rho$ in (23) is replaced by its geostrophic balance form $-\rho_0 f\mathbf{k}\times\mathbf{u}_z/g$ is made, then Eq. (23) can be written in the form

$$f\mathbf{k}\times\mathbf{U}+\nabla p/\rho_0=-\left(\frac{\kappa\rho_0 f^2}{g\rho_z}\mathbf{u}_z\right)_z+\mathbf{X}_z/\rho_0. \quad (24)$$

Equation (24) shows the analogy between the GM90 parameterization and vertical mixing of momentum with a coefficient of $\kappa f^2/N^2$, where N is the buoyancy frequency. This analogy has been discussed previously in Olbers et al. (1985), Greatbatch and Lamb (1990), and McWilliams and Gent (1994). The analogy is not exact because of the approximation made above. If, in addition, $\mathbf{u}_z$ is replaced by $\mathbf{U}_z$ in the first term on the right-hand side of (24), then the kinetic energy and potential energy budgets take the forms

$$\nabla\cdot(p\mathbf{U})+(pW)_z+\left(\frac{\kappa\rho_0^2 f^2}{g\rho_z}\mathbf{U}\cdot\mathbf{U}_z\right)_z$$
$$=-g\rho W+\mathbf{X}_z\cdot\mathbf{U}+\frac{\kappa\rho_0^2 f^2}{g\rho_z}\mathbf{U}_z\cdot\mathbf{U}_z \quad (25)$$

and

$$\frac{D^*}{Dt}(g\rho z)=g\rho W. \quad (26)$$

Comparing (26) with (19) shows that, when using the effective transport velocity, potential energy appears to be conserved except for the exchange with kinetic energy. However, the kinetic energy due to the wind forcing, $\mathbf{X}_z\cdot\mathbf{U}$, is balanced by exchange with potential energy and a negative definite kinetic energy sink due to the vertical friction. Note that the kinetic energy sink in (25) is the same as the potential energy sink in (19) within the two approximations made in deriving (25) from (23). This shows that the GM90 parameterization will give very similar solutions to an adiabatic model using vertical mixing of momentum with coefficient $\kappa f^2/N^2$. We now test this conjecture.

McWilliams and Gent (1994) used these two models to solve for double-gyre wind-forced solutions in a rectangular domain. The discussion above says that the velocity in the vertical momentum mixing model should be interpreted as the effective transport velocity, whereas the velocity in the model with the GM90 parameterization is the large-scale velocity. Both of these models had additional substantial derivative and biharmonic dissipation terms in the momentum equation. However, the solutions obtained in McWilliams and Gent (1994) are steady, and the momentum advection terms are quite small except in the western boundary layers. This suggests that differences between solutions of the two models will show quantitatively the validity of the approximations made in deriving Eq. (25). Figure 5 of McWilliams and Gent (1994) shows the meridional overturning streamfunction for the large-scale velocity from the model with the GM90 parameterization. Their Fig. 13 shows the same streamfunction from the vertical momentum mixing model, which is to be interpreted as the meridional overturning streamfunction for the effective transport velocity. We have calculated the difference between these two streamfunctions, and it is shown in Fig. 1. If our hypothesis is correct, this should be very similar to the meridional overturning streamfunction for the eddy-induced transport velocity ($\mathbf{u}^*$, w^*) from the model with the GM90 parameterization. This is $\int \kappa\rho_y/\rho_z dx$, and it is shown in Fig. 2. Comparison of the figures shows that they are close and the maximum difference between them is about 5% of the range of values in both figures. Thus, the approximations made in deriving (25) are valid to within 5% at most. One

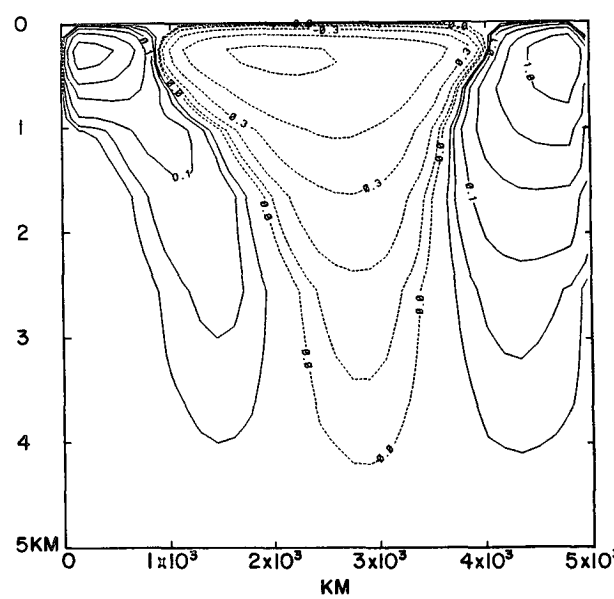

FIG. 1. Zonally averaged meridional overturning streamfunction from the vertical momentum mixing model minus the zonally averaged meridional overturning streamfunction from the model with the GM90 parameterization. The individual streamfunctions are shown in Figs. 13 and 5, respectively, of McWilliams and Gent (1994). Contour intervals are plus and minus $1/32$, $1/16$, $1/8$, $1/4$, $1/2$, and 1 in units of 5×10^4 m^2 s^{-1}.

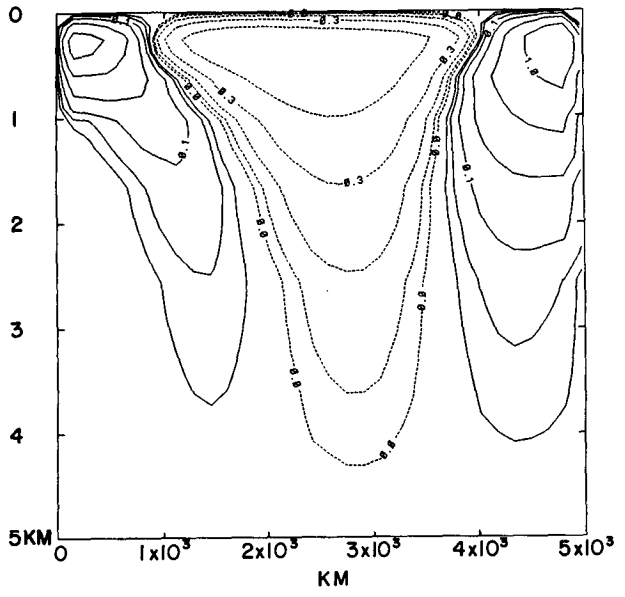

FIG. 2. Zonally averaged meridional overturning streamfunction for the eddy-induced transport velocity, $\int \kappa \rho_y/\rho_z dx$, from the model with the GM90 parameterization described in McWilliams and Gent (1994). Contour intervals and units are the same as Fig. 1.

reason that the streamfunctions are so close is that the kinetic energy input from the wind in the two different calculations in McWilliams and Gent (1994) is almost identical. This can only occur if the velocities in the upper layer are very close. We are unsure whether this is fortuitous in this case, and, in general, perhaps the vertical friction should act on the difference between the total and the Ekman velocities in order to ensure comparable upper-layer velocities and hence comparable kinetic energy input by the wind.

5. Implementation in comprehensive ocean circulation models

Comprehensive ocean circulation models, such as the Cox–Bryan model, usually solve the primitive equations with the Boussinesq approximation. They have prognostic equations for potential temperature θ and salinity S, and both the in situ and potential densities are calculated diagnostically from the equation of state for seawater. Decomposing these variables into low-pass projected large-scale and eddy components gives an equation for large-scale potential temperature of the form

$$\frac{D}{Dt}\bar{\theta} + \nabla\cdot(\overline{\mathbf{u}'\theta'}) + (\overline{w'\theta'})_z = \bar{D}_\theta; \qquad (27)$$

likewise for salinity. In (27) D_θ represents diapycnal processes such as mixing across isopycnals, surface forcing, etc. As discussed at the end of section 1, the eddy flux terms give rise to an advective term due to the skew-symmetric component and a mixing along isopycnals term due to the symmetric tensor component. Thus, the large-scale model equations for θ and S, based on the projection equation (27) and its companion for salinity, are

$$\frac{D^*}{Dt}\theta = R(\mu, \theta) + D_\theta, \qquad (28)$$

$$\frac{D^*}{Dt}S = R(\mu, S) + D_S, \qquad (29)$$

where D^*/Dt and R are defined in (9) and (12), respectively. Calculations of R and the GM90 parameterization for $\mathbf{u}^*$ from (18) require evaluating the slope vector $\mathbf{L}$. In comprehensive models this could be the slope of the in situ density, the global potential density, or the local potential density surfaces. The latter two are defined using a global or local reference pressure, respectively. We think that $\mathbf{L}$ should be the slope of the local potential density, or neutral, surface. The reason is that the constraint of no buoyancy change along neutral surfaces is more fundamental than adiabaticity, which would be preserved if the slope of the global potential density surface were used. We note that, although the GM90 parameterization was strongly guided by quasi adiabaticity and the three properties listed in section 2, these properties are not retained in comprehensive ocean circulation models. The reason is that neutral surfaces are not globally uniquely defined because of the complexities of the equation of state for seawater (see McDougall 1987). Thus, the integrals involved in the properties listed in section 2 are not well defined when they involve neutral surfaces.

Thus, in comprehensive ocean models $\mathbf{L}$ should be evaluated as

$$\mathbf{L} = -\left(\frac{\beta\nabla S - \alpha\nabla\theta}{\beta S_z - \alpha\theta_z}\right) = \frac{(g/\rho)\nabla\rho}{N^2}. \qquad (30)$$

Here α and β are the coefficients of thermal expansion and saline contraction, respectively, which are themselves functions of pressure, θ, and S: $\mathbf{L}$ and R are already implemented in the Cox–Bryan model (see Redi 1982; Cox 1987), so that only an additional advection is required to implement Eqs. (28) and (29). This advection can be done with a similar discretization as already in the model for the large-scale velocity, and numerical conservation properties are retained. In the Cox–Bryan model there is a cutoff in the maximum slope used to evaluate R and a similar cutoff should probably be retained when evaluating the effective transport velocity so that the velocity does not become too large. The Cox–Bryan model uses a second-order accurate leapfrog time differencing scheme, with the advective terms evaluated at the central time level. Computations described in the following section have shown that the GM90 parameterization is numerically unstable if the eddy-induced transport velocity given by (18) is evaluated at the central time level. However,

lagging $\mathbf{u}^*$ one time step so that it is evaluated at the previous time level overcomes this problem. Of course, other time stepping schemes could be used.

6. Relaxation of a sloping two-dimensional front

We now illustrate the effect of the GM90 parameterization by applying it to a strong, sloping two-dimensional front. The front is defined by the initial fields of temperature and salinity that are shown in Fig. 3. The upper right of the front has warm, salty water, and the lower left has cold, fresh water. The initial distributions are of the form

$$\alpha\theta = -\frac{4}{3}\gamma(x, z) + \delta(x, z), \tag{31}$$

$$\beta S = -\frac{1}{3}\gamma(x, z) + \delta(x, z), \tag{32}$$

where γ is a tanh function in z about a center line described by a tanh function in x and δ is a tanh function in x at the upper surface and is very small at the lower surface. Thus, the temperature and salinity partially compensate and the initial density field is given by

$$\rho/\rho_0 = \beta S - \alpha\theta = \gamma(x, z), \tag{33}$$

with α and β constants. This front has a jet in the meridional direction associated with it, but this plays no part in the evolution because all fields are assumed to be independent of y. Thus, the large-scale velocity in the (x, z) plane is identically zero and the only advective component is the eddy-induced transport velocity due to the GM90 parameterization. We have also assumed that there is no mixing of tracers along isopycnals, that is, R in (11) is zero, in order to isolate the advective effect of the parameterization. Then θ and S evolve according to equations

$$\frac{\partial}{\partial t}\theta + (u^*\theta)_x + (w^*\theta)_z = 0, \tag{34}$$

$$\frac{\partial}{\partial t}S + (u^*S)_x + (w^*S)_z = 0, \tag{35}$$

where

$$u^* = \left(\kappa\frac{\rho_x}{\rho_z}\right)_z, \quad w^* = -\left(\kappa\frac{\rho_x}{\rho_z}\right)_x; \tag{36}$$

κ is taken to be a constant except on the boundaries where it is set to zero. This is to satisfy the boundary condition (15). Equations (34) and (35) are solved on a mesh of 40×30 gridpoints as indicated on Fig. 3 using second-order central space and time differencing. As mentioned at the end of section 5, the scheme is unstable if u^* and w^* are evaluated at the central time level, but it is stable when the velocities are evaluated at the previous time level.

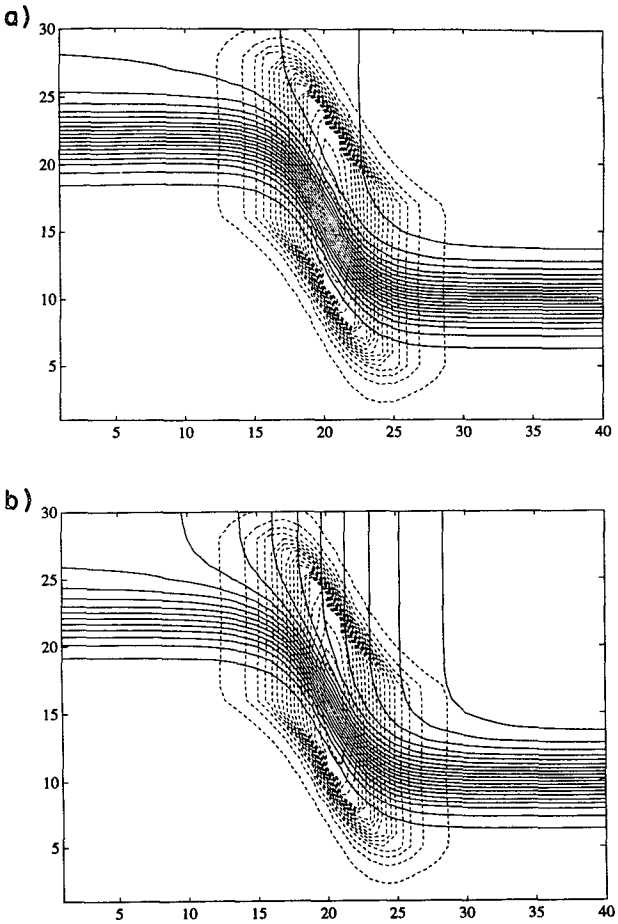

FIG. 3. Initial states of (a) temperature and (b) salt [contour interval one-quarter that of (a)]. Both panels also show the streamfunction $\kappa\rho_x/\rho_z$ for the parameterized eddy-induced transport velocity.

The streamfunction for the velocities defined in (36) is $\kappa\rho_x/\rho_z$, and it is plotted at the initial time by the dotted lines in Fig. 3. It shows that the highest velocities are not at the center of the front but surround it and will produce an anticlockwise circulation that will tend to flatten out the front. Figure 4 shows the temperature and salinity fields at a time of $20\Delta s^2/\kappa$, where Δs is the grid spacing in x and z. Again the dotted lines are the streamfunction for the velocities in (36), with the same contour interval as in Fig. 3. It is clear that the strength of the anticlockwise circulation has decreased significantly by this time because the horizontal density gradient has also decreased. The temperature and salinity distributions above the front now have considerable vertical structure, so that local casts of θ and S have changed considerably compared to their initial distributions. However, the θ–S curves remain smooth all through the integration because the properties of individual parcels are conserved. The θ–S curves from vertical casts in the ocean do show evidence of mutual lateral intrusions of water masses from opposite hori-

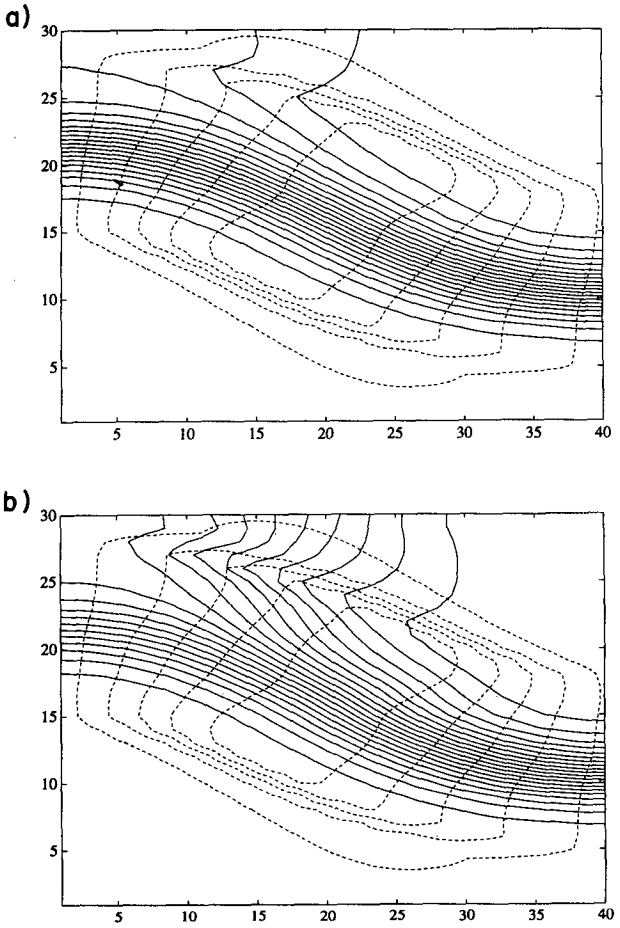

FIG. 4. Distributions of (a) temperature and (b) salt after an integration time of $20\Delta s^2/\kappa$. Both panels also show the streamfunction $\kappa\rho_x/\rho_z$ for the parameterized eddy-induced transport velocity. Contour intervals are the same as in Fig. 3.

zontal directions as the thickness along isopycnals is made more uniform by lateral advections of fluid and tracer.

The integration has been continued to equilibrium. Figure 5 shows the initial density field, the density at time $20\Delta s^2/\kappa$ corresponding to Fig. 4 and at time $1000\Delta s^2/\kappa$ when it has reached equilibrium. It is clear that the GM90 parameterization acts to flatten the front, and the final state is that the front is horizontal. This corresponds to a state of minimum potential energy as is expected from (19). However, the vertical stratification has remained intact, so that the amount of water of a given density is unchanged to within numerical discretization accuracy. This is to be expected from the quasi-adiabatic character of the parameterization, but it is encouraging that this conservative behavior is maintained in a calculation on a coarse Cartesian grid with its unavoidable numerical dispersion errors. These properties are certainly not retained if the parameterization of eddy effects is just horizontal diffusion of tracers rather than (34) and (35). We calculated the effect of horizontal diffusion on the initial front shown in Fig. 5, and the equilibrium state is much more diffuse in the vertical than that shown in Fig. 5. Using the GM90 parameterization in ocean general circulation models enables the coefficient of horizontal

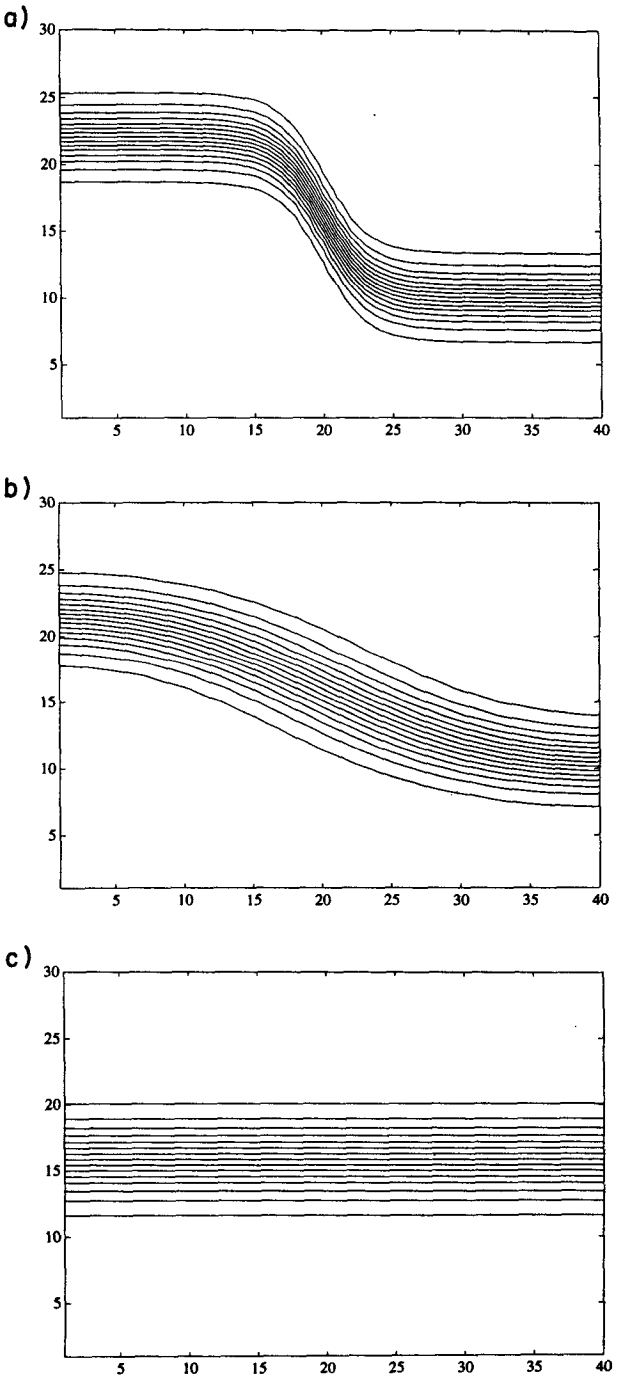

FIG. 5. Density distribution at various times of the integration. (a) Initial, (b) $20\Delta s^2/\kappa$, and (c) $1000\Delta s^2/\kappa$.

diffusion of tracers to be set to zero, as in McWilliams and Gent (1994).

7. Estimates using ocean data

We now illustrate the effects of the GM90 parameterization by some estimates using the Levitus (1982) dataset. This dataset is very frequently used to initialize and validate ocean numerical models. The zonal mean meridional overturning streamfunction for the eddy-induced transport velocity is the zonal integral of κ times the meridional component of the slope vector $\mathbf{L}$, calculated from (30). This streamfunction is shown in Fig. 6 using a constant value for the thickness diffusivity κ of 10^3 m^2 s^{-1} and imposing zero values of the streamfunction on the boundaries. It has been calculated over all the ocean basins with a resolution of 4° in latitude and 200 m in depth. The value chosen for κ is a standard value for horizontal tracer mixing in the Cox–Bryan model.

The strongest cell in the Northern Hemisphere is centered at 40°N between 200 and 400 m and corresponds to a transport of 4 Sv (Sv $\equiv 10^6$ m^3 s^{-1}). This cell is fairly equally divided between the North Atlantic and North Pacific Oceans. By far the largest signal is in the region of the Antarctic Circumpolar Current where there is a transport of 18 Sv in an overturning cell between depths of 0.5 and 2.5 km. The implied circulation is around this depth range between 52°S and 56°S. The meridional velocities are confined to above 500 m and below 2.5 km. Between these two depths, the isopycnals do have a significant slope, but the slope is constant with depth so that the meridional velocity is zero. In fact, the isopycnals have the same slope right to the surface in this latitude range, so it is the imposition of the boundary condition $w^* = 0$ at the surface that forces the meridional velocity to be surface intensified. To a degree the same thing occurs in the deep ocean but, because there is a range of ocean depths, the intensification is less apparent in Fig. 6. The vertical velocity in the overturning cell is mostly confined to 40°–48°S and 60°–64°S on both sides of the average latitude of the Antarctic Circumpolar Current.

This discussion leads to the following thought experiment. Consider a situation where the isopycnals have a constant slope throughout a rectangular domain. Then a parameterization for the eddy-induced transport velocity based on the downgradient flux of thickness will have no effect at all, providing the constant isopycnal slope is imposed at all boundaries. Then the first and third terms on the right-hand side of the potential energy budget (19) cancel exactly and this configuration will persist indefinitely. However, if the McWilliams and Gent (1994) boundary condition implementation, described below Eq. (19), is used, then there will be an eddy-induced circulation near the boundaries that will eventually flatten the isopycnals. In this case the internal sink term in (19) will reduce the potential energy to its minimum value when the isopycnals are flat. This emphasizes that, at an open boundary, the appropriate boundary condition is to specify a nonzero normal component of $\kappa\mathbf{L}$. In a general situation, isopycnals will have slopes at closed boundaries even with the McWilliams and Gent (1994) implementation of the boundary conditions. This will

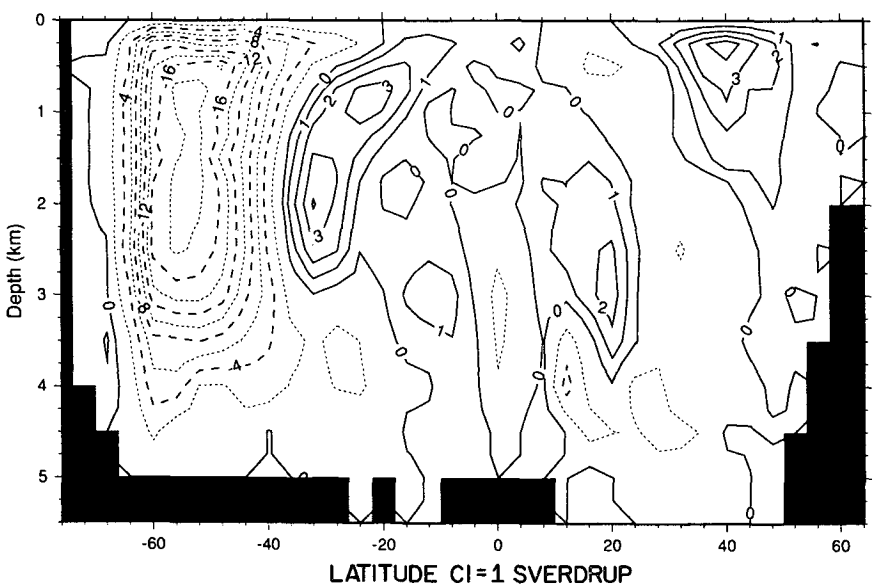

FIG. 6. Zonally averaged meridional overturning streamfunction $\int \kappa\rho_y/\rho_z dx$ in Sverdrups calculated from Levitus (1982) data where the average is over all ocean basins: $\kappa = 10^3$ m^2 s^{-1} and is constant.

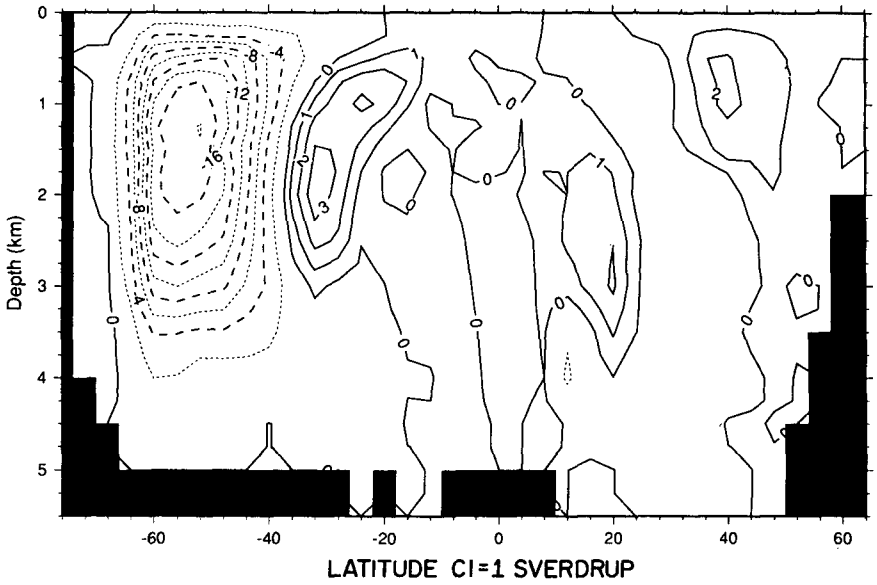

FIG. 7. Zonally averaged meridional overturning streamfunction in Sverdrups as in Fig. 6 but for κ with a first baroclinic mode profile.

occur when either large-scale advection or diabatic processes counterbalance the effects of the eddy-induced transport velocity at the boundary.

In some of their solutions McWilliams and Gent (1994) used profiles of κ that were tapered to zero over several horizontal grid points near side boundaries. This was to diminish the intensification of velocities at side boundaries due to the GM90 parameterization. Tapering the vertical profile of κ to zero at the top and bottom boundaries has a similar benefit. Here we examine the effects of choosing a vertical profile for κ based on the vertical velocity profile of the first baroclinic mode for the Antartic Circumpolar Current region. It is zero at the upper and lower boundaries and has a maximum of one at 0.3 of the ocean depth. This profile was used globally and the meridional overturning streamfunction recalculated from the Levitus (1982) data. It is shown in Fig. 7. Compared to Fig. 6, the maximum in the streamfunction in the Antartic Circumpolar Current is only reduced slightly, but its vertical and horizontal extent is reduced so that the circulation is much less boundary intensified.

The largest effect of using a tapered vertical profile for κ is on the heat transport implied by the eddy-induced transport velocity. This has been calculated using the temperatures from the Levitus data and is shown in Fig. 8 when κ is constant at 10^3 m^2 s^{-1}. The heat transport when κ has a tapered vertical profile is very similar in shape but has almost exactly one-half the values shown in Fig. 8. This is to be expected as the constant κ case forces the circulation to be shallow and deep in the ocean and so maximizes the heat transport. Figure 8 shows the northward heat transport in petawatts plotted as a function of latitude calculated for the total ocean and also shows the contributions by the Atlantic and Pacific Oceans individually. All three curves show the same general features of equatorward heat transport between 25°N and 20°S and poleward heat transport north of 32°N and south of 28°S. The direction and magnitude of this heat transport is consistent with the effect of eddies estimated from observations and calculated in regional models of ocean circulation. Near the equator 20–30-day waves are observed in all oceans, especially in the eastern Pacific. They transport heat equatorward down the mean tem-

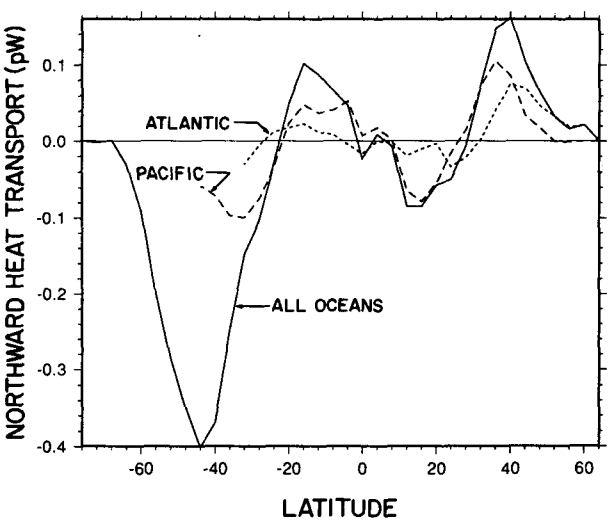

FIG. 8. Northward heat transport in petawatts due to the streamfunction shown in Fig. 6 calculated from Levitus (1982) data. The heat transports in the Atlantic, Pacific, and all ocean basins are shown.

perature gradient (see Bryden and Brady 1989; Brady and Gent 1994). In the North Atlantic eddies transport heat polewards (see Bryan and Holland 1989; Beckmann et al. 1994). In Fig. 8 the maximum transport in the Northern Hemisphere is 0.15 petawatts at 40°N, which is consistent in magnitude with the regional model eddy heat transports. The maximum in the Southern Hemisphere in Fig. 8 is 0.4 petawatts at 44°S, consistent with the effect of eddies estimated from observations (see Bryden 1979; de Szoeke and Levine 1981) and the FRAM model (see Webb 1993). This value is reduced to 0.2 petawatts when κ has the smooth first baroclinic mode profile.

Further detailed comparison of Fig. 8 with observations and models is not warranted. Suffice it to say that the GM90 parameterization with κ of order 10^3 $m^2\ s^{-1}$ can provide an ocean heat transport by eddies that is the same order of magnitude and has the correct distribution with latitude as estimates from observations and regional eddy-resolving models. The detailed structure of this heat transport will depend on the horizontal and vertical structure chosen for κ. The best choice for κ as a function of x, y, and z is a research question beyond the scope of this manuscript.

8. Summary and conclusions

Section 2 shows how the effect of eddies can be parameterized in a large-scale numerical ocean model. This is accomplished by mixing tracers along local potential density, or neutral, surfaces and advecting them by the effective transport velocity. This velocity is the sum of the large-scale velocity plus the parameterized eddy-induced transport velocity. Any choice can be made for this eddy-induced transport velocity providing it satisfies the usual continuity equation and boundary condition of no normal flow. This choice could be based on analyses of eddy-resolving calculations. Section 3 discusses the GM90 parameterization for the eddy-induced transport velocity based on nearly downgradient diffusion of thickness. This parameterization mimics the domain-averaged effect of baroclinic instability in that it provides a negative definite sink of large-scale potential energy. Thus, a consistent way to estimate the thickness diffusivity κ is by comparison to the large-scale potential energy loss to eddy potential energy in adiabatic eddy-resolving calculations. We have used a value of 10^3 $m^2\ s^{-1}$ in this paper; McWilliams and Gent (1994) used 1.5×10^3 $m^2\ s^{-1}$. There is an additional coefficient μ in the mixing along neutral surfaces term and this need not be equal to κ. Instead it represents the amount of stirring done by eddies and so it could be estimated by a mixing length argument as an eddy velocity scale times an eddy length scale. Alternatively, it could be proportional to eddy kinetic energy divided by a mixing time estimated from observations or from eddy-resolving models.

In section 4 the planetary geostrophic momentum equation is formulated in terms of the effective transport velocity. The conclusion is that the effective transport velocity using the GM90 parameterization is very similar to the large-scale velocity from an adiabatic model using vertical mixing of momentum with a coefficient of $\kappa f^2/N^2$. Section 5 is a discussion of how to implement the eddy-induced transport velocity in comprehensive primitive equation models, such as the Cox–Bryan model. The additional advection should be implemented in a similar manner to the large-scale velocity advection. If central time differencing is used, however, then the eddy-induced transport velocity must be evaluated at the previous, not central, time level.

Application of the GM90 parameterization to a two-dimensional sloping front is presented in section 6. It shows that the conservative properties of the parameterization are well-maintained on a Cartesian grid and that the parameterization works very much better than horizontal diffusion in maintaining the amount of water with a given density. Section 7 shows estimates from Levitus (1982) data of the meridional overturning streamfunction and associated heat transport due to the eddy-induced transport velocity. The conclusion is that, with κ of order 10^3 $m^2\ s^{-1}$, the parameterized eddy ocean heat transport is the same order of magnitude and has the correct distribution with latitude as estimates from observations and regional eddy-resolving models.

Further evaluation of the GM90 parameterization will only come from implementing it in ocean numerical models, and early results are described in Danabasoglu et al. (1994) and Böning et al. (1995). The optimal form of κ as a function of position is a question to be addressed during this implementation. Other parameterizations should also be tried, but the way to formulate them in terms of the eddy-induced transport velocity presented in this paper is the natural method to follow.

Acknowledgments. Nancy Norton (NCAR) performed the calculations for Figs. 1 and 2, and David Jackett (CSIRO) produced Figs. 6, 7, and 8. The work in this manuscript was undertaken while the first two authors were on extended visits to the CSIRO Marine Laboratories in Hobart. It was written while the first author was visiting the Centre for Dynamical Meteorology at Monash University, Melbourne. NCAR is sponsored by the National Science Foundation.

APPENDIX

General Vertical Coordinate

With the GM90 parameterization, the tracer equation (11) in any vertical coordinate s can be written in the form

$$\frac{D^*}{Dt}\tau = R(\mu, \tau), \qquad \text{(A1)}$$

where D^*/Dt is defined by

$$\frac{D^*}{Dt} = \frac{\partial}{\partial t} + (\mathbf{u} + \mathbf{u}^*)\cdot\nabla_s + (\omega + \omega^*)\frac{\partial}{\partial s}; \quad \text{(A2)}$$

D^*/Dt can also be written in the form

$$\frac{D^*}{Dt} = \frac{D^*t}{Dt}\frac{\partial}{\partial t} + \frac{D^*\mathbf{x}}{Dt}\cdot\nabla_s + \frac{D^*s}{Dt}\frac{\partial}{\partial s}. \quad \text{(A3)}$$

The eddy-induced transport velocity $(\mathbf{u}^*, \omega^*)$ is defined by

$$h_s\mathbf{u}^* = -[\kappa(\nabla_s h + h_s\mathbf{S})]_s, \quad h_s\omega^* = \nabla_s\cdot[\kappa(\nabla_s h + h_s\mathbf{S})], \quad \text{(A4)}$$

where h is the physical height of an s surface, and $\mathbf{S}$ is defined by

$$\mathbf{S} = -\nabla_s\rho/\rho_s. \quad \text{(A5)}$$

The continuity equation for the eddy-induced transport velocity is

$$\nabla_s\cdot(h_s\mathbf{u}^*) + (h_s\omega^*)_s = 0. \quad \text{(A6)}$$

In the s vertical coordinate, $R(\mu, \tau)$ takes the form

$$R(\mu, \tau) = \nabla_s^{3D}\cdot[\mu h_s\mathbf{K}\nabla_s^{3D}\tau]/h_s, \quad \text{(A7)}$$

where

$$\mathbf{K} = \begin{pmatrix} \mathbf{I} & \mathbf{S} \\ \mathbf{S} & \mathbf{S}\cdot\mathbf{S} \end{pmatrix}, \quad \nabla_s^{3D} = \left(\nabla_s, \frac{\partial}{\partial s}\right). \quad \text{(A8)}$$

REFERENCES

Andrews, D. G., 1990: On the forcing of time-mean flows by transient, small-amplitude eddies. *J. Atmos. Sci.*, **47**, 1837–1844.

——, and M. E. McIntyre, 1978: An exact theory of nonlinear waves on a Lagrangian flow. *J. Fluid Mech.*, **89**, 609–646.

——, J. R. Holton, and C. B. Leovy, 1987: *Middle Atmosphere Dynamics.* Academic Press, 489 pp.

Beckmann, A., C. W. Böning, C. Köeberle, and J. Willebrand, 1994: Effects of increased horizontal resolution in a simulation of the North Atlantic Ocean. *J. Phys. Oceanogr.*, **24**, 326–344.

Böning, C. W., W. R. Holland, F. O. Bryan, G. Danabasoglu, and J. C. McWilliams, 1995: An overlooked problem in model simulations of the thermohaline circulation and heat transport in the Atlantic Ocean. *J. Climate*, **8**, 515–523.

Brady, E. C., and P. R. Gent, 1994: The seasonal cycle of meridional heat transport in a numerical model of the Pacific equatorial upwelling zone. *J. Phys. Oceanogr.*, **24**, 2658–2673.

Bryan, F. O., and W. R. Holland, 1989: A high resolution simulation of the wind and thermohaline driven circulation in the North Atlantic Ocean. *Parameterization of Small Scale Processes,* P. Muller and G. Holloway, Eds., *Proc. Fourth 'Aha Huliko'a Hawaiian Winter Workshop,* University of Hawaii at Manoa, 99–115.

Bryden, H. L., 1979: Poleward heat flux and conversion of available potential energy in Drake Passage. *J. Mar. Res.*, **37**, 1–22.

——, and E. C. Brady, 1989: Eddy momentum and heat fluxes and their effects on the circulation of the equatorial Pacific Ocean. *J. Mar. Res.*, **47**, 55–79.

Cox, M. D., 1987: Isopycnal diffusion in a z-coordinate ocean model. *Ocean Model.*, **74**, 1–5.

Csanady, G. T., 1989: Energy dissipation and upwelling in a western boundary current. *J. Phys. Oceanogr.*, **19**, 462–473.

Danabasoglu, G., J. C. McWilliams, and P. R. Gent, 1994: The role of mesoscale tracer transports in the global ocean circulation. *Science*, **264**, 1123–1126.

Davis, R. E., 1994: Diapycnal mixing in the ocean: Equations for large-scale budgets. *J. Phys. Oceanogr.*, **24**, 777–800.

de Szoeke, R. A., and M. D. Levine, 1981: The advective flux of heat by mean geostrophic motions in the Southern Ocean. *Deep-Sea Res.*, **28**, 1057–1085.

——, and A. F. Bennett, 1993: Microstructure fluxes across density surfaces. *J. Phys. Oceanogr.*, **23**, 2254–2264.

Gent, P. R., and J. C. McWilliams, 1990: Isopycnal mixing in ocean circulation models. *J. Phys. Oceanogr.*, **20**, 150–155.

Greatbatch, R. J., and K. G. Lamb, 1990: On parameterizing vertical mixing of momentum in non-eddy-resolving ocean models. *J. Phys. Oceanogr.*, **20**, 1634–1637.

Levitus, S., 1982: *Climatological Atlas of the World Ocean.* NOAA Prof. Paper No. 13, U.S. Dept. Commerce, Washington, DC, 173 pp.

McDougall, T. J., 1987: Neutral surfaces. *J. Phys. Oceanogr.*, **17**, 1950–1964.

——, 1991: Parameterizing mixing in inverse models. *Dynamics of Oceanic Internal Gravity Waves,* P. Muller and D. Henderson, Eds., *Proc. Sixth 'Aha Huliko'a Hawaiian Winter Workshop,* University of Hawaii at Manoa, 355–386.

——, and J. A. Church, 1986: Pitfalls with the numerical representation of isopycnal and diapycnal mixing. *J. Phys. Oceanogr.*, **16**, 196–199.

McWilliams, J. C., and P. R. Gent, 1994: The wind-driven ocean circulation with an isopycnal-thickness mixing parameterization. *J. Phys. Oceanogr.*, **24**, 46–65.

Middleton, J. F., and J. W. Loder, 1989: Skew fluxes in polarized wave fields. *J. Phys. Oceanogr.*, **19**, 68–76.

Olbers, D. J., M. Wenzel, and J. Willebrand, 1985: The inference of North Atlantic circulation patterns from climatological hydrographic data. *Rev. Geophys. Space Phys.*, **23**, 313–356.

Plumb, R. A., 1986: Three-dimensional propagation of transient quasi-geostrophic eddies and its relationship with the eddy forcing of the time-mean flow. *J. Atmos. Sci.*, **43**, 1657–1678.

——, 1990: A nonacceleration theorem for transient quasigeostrophic eddies on a three-dimensional time-mean flow. *J. Atmos. Sci.*, **47**, 1825–1836.

——, and J. D. Mahlman, 1987: The zonally averaged transport characteristics of the GFDL general circulation–transport model. *J. Atmos. Sci.*, **44**, 298–327.

Redi, M. H., 1982: Oceanic isopycnal mixing by coordinate rotation. *J. Phys. Oceanogr.*, **12**, 1154–1158.

Rhines, P. B., 1982: Basic dynamics of the large-scale geostrophic circulation. Summer Study Program in Geophysical Fluid Dynamics, Woods Hole Oceanographic Institution, 1–47.

Webb, D. J., 1993: FRAM—the UK fine resolution Antarctic model. *Proc. 4th International Conf. on Southern Hemisphere Meteorology and Oceanography,* Australian Meteorological Society, 152 pp.